Sustainable Energy & Fuels

ROYAL SOCIETY OF CHEMISTRY

PAPER

View Article Online
View Journal | View Issue

Cite this: *Sustainable Energy Fuels*, 2026, **10**, 2110

A corrosion study of lithium-ion batteries during NaCl electrochemical discharge: mechanistic origins and Zn-based mitigation strategies

Hanna Sahivirta, [a] Annukka Santasalo-Aarnio[b] and Rodrigo Serna-Guerrero*[a]

As lithium-ion battery (LIB) demand increases, there is growing interest in their recycling to reduce the environmental impact of mining. The safe handling of end-of-life batteries during transportation, storage and mechanical treatment requires development of environmentally sustainable and industrially scalable discharging processes. In this context, electrochemical discharge shows promise due to its simplicity, robustness, and potentially low cost. NaCl solution has been extensively studied as a promising discharge medium because of its availability and reportedly fast discharge potential. However, the use of NaCl aqueous electrolyte solutions has resulted in casing corrosion, which is associated with inefficient discharge and losses of critical raw materials. To overcome these issues, the present study offers for the first time an in-depth exploration of the potential mechanisms responsible for LIB corrosion in NaCl solutions. It is found that corrosion is a consequence of multiple parallel reactions driven by the presence of dissolved oxygen produced during electrochemical water splitting. As the corrosion pathways are identified, a novel approach is proposed to prevent it, namely, the use of Zn-salts as corrosion inhibitors. The experimental results suggest that Zn^{2+} ions aid in corrosion prevention in three main ways: (i) by forming non-soluble $Zn(OH)_2$ with OH^- ions produced on the metal surfaces; (ii) by forming mixed Fe–Zn oxide in corrosion pits; and (iii) by consuming electrons from the battery during discharge and forming a sacrificial anode of metallic Zn. The present work thus proposes an economical and reliable approach to discharge LIBs efficiently using aqueous electrolyte media.

Received 3rd January 2026
Accepted 11th March 2026

DOI: 10.1039/d6se00009f

rsc.li/sustainable-energy

1 Introduction

Lithium-ion batteries (LIBs) largely power the electrification and digitalization of society with applications ranging from energy storage systems to electric vehicles, telecommunications, robotics, portable medical devices and household tools. However, the rapid increase in the demand for LIB-powered devices also raises concerns about the availability of raw materials needed for their manufacturing, the ethics of critical mineral production, and the environmental impact of the entire life cycle of LIBs.[1] For instance, according to the EU battery regulatory framework, 70% of the LIB materials need to be recycled from 2030 onwards to aid in reducing the exploitation of virgin raw material sources.[2]

It is widely acknowledged that the high reactivity of LIB active electrode materials and the presence of volatile and flammable components represent significant safety risks during dismantling, collection, transportation, and storage. Short circuits caused by unintentional contact between the positive and negative battery poles during transportation and storage and the subsequent exposure of highly combustible Li/Li^+ to ambient oxygen during crushing lead to fires, explosions, and production of toxic gas emissions.[3–5] Recycling methods involving the mechanical and hydrometallurgical treatment of LIBs require extensive crushing of spent LIB cells to liberate the recyclable materials from the battery structure. The recyclability of valuable materials is compromised after combustion due to material loss and contamination.[4] While the importance of discharging is well established, the research focusing on this issue requires systematic development.

An economically sensible discharge process should allow the treatment of various types of batteries in bulk. The published literature suggests two options for scalable discharging methods: immersion of battery cells in an electrolyte solution or burying them in conducting powder. Discharge in conductive powder is fast and considered cleaner, although it results in a sharp rise in temperature and the risk of thermal runaway.[4,6,7] Yao *et al.*[7] concluded that graphite powder has the risk of dust explosion, while metal powders, especially copper, oxidize easily. Oxidized metals have lower conductivity and thus this system is likely to waste valuable metal resources. Alternatively,

[a]*Department of Chemical and Metallurgical Engineering (CMET), School of Chemical Engineering, Aalto University, Vuorimiehentie 2, Espoo, 02150, Finland. E-mail: rodrigo.serna@aalto.fi*

[b]*Research Group of Energy Conversion and Systems, Department of Energy and Mechanical Engineering, School of Engineering, Aalto University, PO Box 14400, FI-00076 AALTO, Finland*

stainless steel powder could have better durability although this does not solve the issue of high temperature generation.

For the reasons presented above, electrochemical discharge using aqueous salt solutions has gained attention as a simple, scalable discharging method. In aqueous NaCl solutions, the simultaneous reactions of water splitting (reaction 1) and Cl_2 gas formation (reaction 2) consume electrical energy from the battery while any heat released can be absorbed by the aqueous solution, reducing the risk of thermal runaway.[6,8–13]

$$2H_2O(l) \rightarrow 2H_2(g) + O_2(g)\ E^\circ = 1.23\ V \quad (1)$$

$$2Cl^- \rightarrow Cl_2 + 2e^-\ E^\circ = 1.36\ V \quad (2)$$

Admittedly, submerging batteries in aqueous salt solutions also presents its own set of challenges. Voltage relaxation is a well-documented phenomenon where, as the battery is removed from the salt solution, its charge increases spontaneously, preventing the accurate evaluation of the state of charge (SOC).[13,14] This means that electrochemically discharged batteries do not reflect the actual voltage that the battery will have after relaxation and may not be as safe to transport and recycle as they would appear. The second significant challenge is the corrosion of the battery terminals and casing, potentially releasing internal battery components into the discharge solution and resulting in process water contamination.[6–16] The loss of critical and strategic raw materials such as Co, Li, Cu, Ni, and Al already during the discharging step creates further challenges to reach the ambitious recovery targets set by the EU.[2] Corroded battery terminals can also prevent the proper discharge of the battery and may be responsible for faulty SOC readings.[10,13]

Since the duration and low cost of battery discharge methods are important factors for their industrial-scale application, NaCl solution is the most extensively studied discharge medium for LIBs. NaCl solutions are considered highly conductive, therefore presenting a fast discharge rate, as well as relatively mild voltage relaxation behaviour of the final voltage, which remained below 2 V. However, it is well documented that NaCl solution results in a fast corrosion rate of the battery terminals and casing.[6–16] Consequently, research has focused on finding alternative discharge media to address these concerns.

Among the most frequently studied non-corrosive alternatives to replace NaCl are solutions of sulphate salts such as $ZnSO_4$,[8,17] $MnSO_4$,[7,9,15,18] $MgSO_4$,[12,15] solutions of carbonates like Na_2CO_3 and K_2CO_3,[6,13,16] ammonia-based electrolytes[14,16] and acetates.[9] However, corrosive effects of varying severity have been observed with discharging studies, including sulphate solutions of Na_2SO_4,[6,8,16–18] $FeSO_4$,[7–9,17,19] $CuSO_4$ (ref. 19) and alkaline solutions such as NaOH.[11,16,18] Evidently, the discharge efficiency of different salt solutions varies greatly depending on the electrochemical behaviour of the chemical species in the solution, their concentration, solubility and the resulting conductivity of the solution. In most cases, fast discharging rates are accompanied by corrosion damage to the battery, and the non-corrosive alternatives so far explored result in slow discharge that does not reach a safe level for recycling.

While corrosion is a well-recognized issue during the electrochemical discharge of LIBs, the corrosion mechanisms of the battery terminals and casing structures have not been thoroughly studied. Indeed, most studies have limited their analysis to a visual evaluation of the extent of corrosion.[8,11,13,16,18] Other studies have quantified corrosion products present in the discharge solutions by inductively coupled plasma (ICP) analysis, however measuring only the extent of metal loss rather than providing a detailed analysis of the mechanisms responsible for corrosion.[6,7,9,17,19]

In an attempt to address the limitations of aqueous salt solutions as battery discharge media, the present study has two main objectives: (i) unveil the mechanisms responsible for the corrosion of LIB casing materials, and (ii) exploit this fundamental understanding to identify appropriate methods for corrosion prevention. As will be explained in the subsequent sections, the proposed method hereby proposed consists of the use of Zn-containing salts as corrosion inhibitors which, to the best of the authors' knowledge, is an approach that has never before been tested in this field. Finally, the experimental results of discharge in the presence of Zn-salts were rationalized to propose corrosion prevention mechanisms.

2 Materials and experimental methods

2.1 Minerals and reagents

The discharging experiments in this work were conducted using new cylindrical LIBs type $LiNi_xMn_yCo_z$ (NMC; Samsung 18 650 INR18 650-25R, 2500 mAh, South Korea) without a protective circuit. The batteries had a nominal voltage of 3.6 V.

All electrolyte solutions were prepared using ultra-high purity water (15 MΩ cm, purified by Purelab, Elga, High Wycombe, UK) and different concentrations of NaCl (S9888, Merck (Sigma-Aldrich, Finland)), $ZnCl_2$ (208 086, Merck (Sigma-Aldrich, Finland)) and $ZnSO_4 \cdot 7H_2O$ (221 376, Merck (Sigma-Aldrich, Finland)) according to Table 1. Solutions containing only NaCl were prepared to identify the corrosion mechanisms of the battery casing during discharge. This was followed by solutions containing $ZnCl_2$ and $ZnSO_4 \cdot 7H_2O$ as corrosion inhibitors.

2.2 Discharging procedure

The batteries were discharged by submerging them into a glass beaker containing the electrolyte solution under continuous mixing using a magnetic stirrer. Mixing the discharge solution reduces the time for chlorine to attack the metal surfaces.[20]

The voltage change during discharging was measured by removing the battery from the solution at specific time intervals and connecting to a Fluke 287 True-RMS Electronics Logging Multimeter (Everett, Washington, USA). This procedure was performed until the voltage could not be visibly reduced. The voltage relaxation behaviour was monitored with the same instrument over 24 h after the discharging experiment. A Mettler Toledo SevenExcellence™ multi-channel pH meter (Greifensee, Switzerland) was used to monitor the electrolyte

Table 1 Electrolyte compositions and concentrations of Li-ion battery discharge solutions

Solution concentration m (mol kg^{-1})
0.15 m NaCl
1 m NaCl
1 m NaCl + 0.3 m $ZnCl_2$
1 m NaCl + 0.3 m $ZnSO_4$
3 m NaCl + 2.5 m $ZnSO_4$
1.75 m NaCl + 1.55 m $ZnSO_4$
0.5 m NaCl + 3 m $ZnSO_4$

solution, providing information on electrochemical reactions in the solution as a function of time. Reaction byproducts formed a precipitate at the bottom of the beaker which was collected and dried for further analysis. A schematic diagram of the experimental setup is shown in Fig. 1.

2.3 Characterization of batteries and precipitate

After the discharging experiments, batteries were cooled with liquid nitrogen to allow their safe disassembly. The batteries were sawed in half inside a glovebox filled with Ar gas. The section with the positive battery terminal was cast in epoxy to prepare a metallographic cross section for scanning electron microscopy (SEM) and energy dispersive X-ray spectroscopy (EDS) analysis using a SEM-EDS, MIRA3 SEM, Tescan, Brno, Czech Republic and UltraDry Silicon Drift energy dispersive X-ray spectrometer. The cross sections were polished with SiC-papers P80, P240, P400, P800, P1200, and P4000 in the same order. The final stages of the polishing were done using velvet polishing discs with 3 μm and 1 μm diamond suspensions. The polished samples were washed in ethanol in an ultrasonic bath for 15 min, after which the cross sections were coated with carbon. The SEM images were obtained with a 15 kV acceleration voltage and back scattered electron detector. EDS analyses were obtained using mineral standards by Astimex Scientific (Toronto, Ontario, Canada).

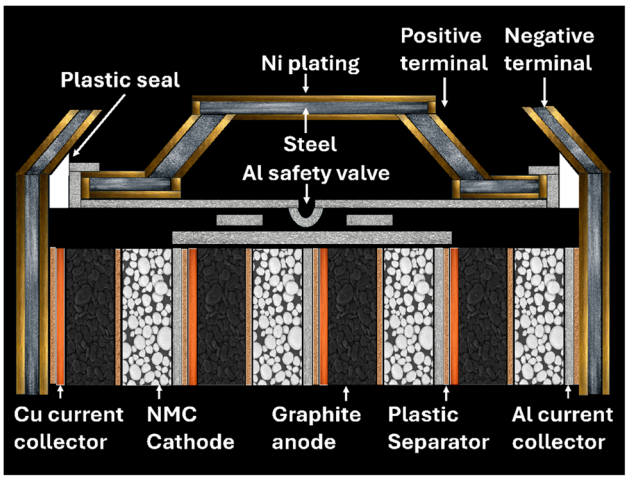

Fig. 2 Schematic diagram of a cylindrical LIB cell cross section.

3 Results and discussion

3.1 Corrosion mechanisms

The corrosion mechanisms of the discharged LIBs were studied by analysing the corrosion patterns and deposits formed on the metal surfaces of the positive terminal. Fig. 2 presents a schematic diagram of a typical LIB cell cross-section for reference in the following discussions. The positive terminal of the LIB cells used in this study consists of a Ni-plated carbon steel structure, beneath which a safety valve made from an alloy (Al–Mg–Fe) is found. The casing consists of Ni-plated carbon steel acting as

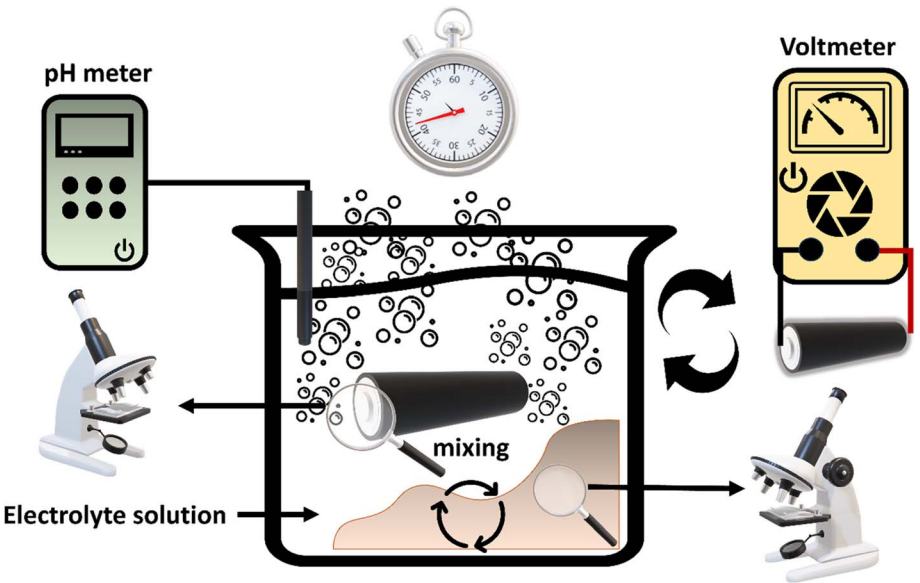

Fig. 1 Schematic diagram of the experimental setup for battery discharging.

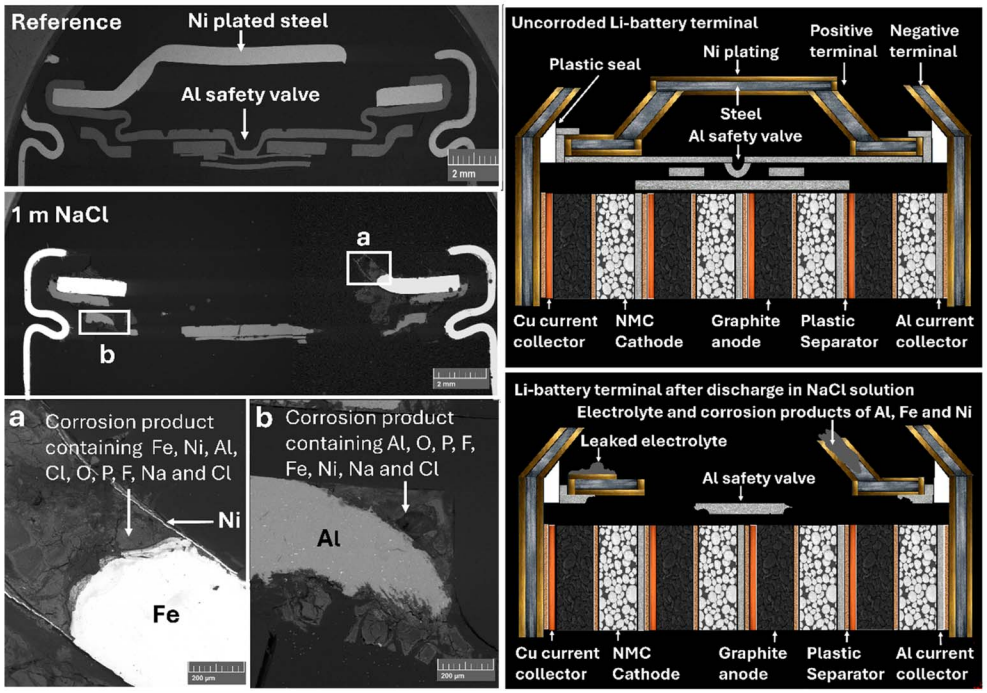

Fig. 3 SEM images of a LIB positive terminal cross section obtained after 3 h discharge in 1 m NaCl solution and schematic diagrams of the LIB cross sections representing uncorroded and corroded cross sections after discharge in NaCl solution. The non-corroded reference cross section was discharged with resistors.

a negative terminal. Electrical isolation between the terminals is ensured by a plastic sealing ring, which insulates the positive terminal from the casing.

In a typical discharge operation with aqueous electrolyte, corrosion was more prominent in the positive terminal. This agrees with the basic principles of corrosion, where metal surfaces acting as cathodes (*i.e.* presenting negative charge) are protected from corrosion. Additionally, negative ions responsible for corrosion (*e.g.* Cl^-) are repelled from the negatively charged surface.[21]

To elucidate the corrosion mechanisms, discharging experiments were performed in 1 m NaCl aqueous solution to obtain samples for SEM-EDS analysis. Fig. 3 shows representative micrographs where it is seen that the positive terminal has almost completely disappeared during discharging, in stark comparison with the non-corroded reference sample discharged with resistors. The remaining pieces of the positive terminal and the safety valve were covered by a deposit containing species that could not be identified with EDS, as shown in the SI (Table S1). This indicates that the deposit contains elements with low atomic mass, potentially from electrolyte leakage as it contains Li and hydrocarbons. It is likely that leaked electrolyte mixed with the corrosion products of Al, Fe and Ni as the positive terminal disintegrates, forming deposits in the crevices of the battery terminal. This conclusion can be further validated by the species that were detected through EDS analysis, showing that the deposit contains Fe, Ni, Al, O, P and F. The source of phosphorus and fluorine is most likely the conducting salt (*i.e.*, $LiPF_6$) in the battery electrolyte.

An additional discharging experiment was performed at a lower NaCl concentration of 0.15 m since the fast corrosion rate of the battery terminal in 1 m NaCl solution resulted in insufficient material left for EDS analysis. The purpose of this experiment was to create conditions where the corrosion rate would be slow enough to preserve information regarding the corrosion mechanism. Consequently, the total discharging time required was longer (*i.e.*, 23 hours) than with 1 m solutions. As shown in Fig. 4, the low NaCl concentration did not prevent the corrosion of the positive terminal. The EDS analysis of the oxide scale formed on the steel surface in Fig. 4b matches well with oxides of FeO(OH), $Fe(OH)_3$, Fe_2O_3 and Fe_3O_4, containing small quantities of Ni, Al, P, Cl and Na, while the reaction product formed on the Al surface in Fig. 4a indicates the formation of a mixture of aluminium hydroxides, fluorides and phosphates. Due to space limitations, the complete EDS analyses of the corrosion products of all NaCl discharging experiments are provided in Table S1 in the SI.

SEM images of the dried precipitate collected from the NaCl discharge experiments are shown in Fig. 5. The EDS analysis of the dried precipitate (Table S1, SI) indicates formation of $Al(OH)_3$ and oxides of Fe, Al and Ni.

3.1.1 Corrosion mechanism of the Ni-plated steel terminal. The species identified in the SEM-EDS analysis can serve as guidelines to determine the electrochemical mechanisms responsible for corrosion of the Ni-plated steel positive terminal, collected in Table 2 and explained next. In addition, Fig. S1–S5 in the SI were used as guidelines to support phase identification. In general, the corrosion of metals in aqueous

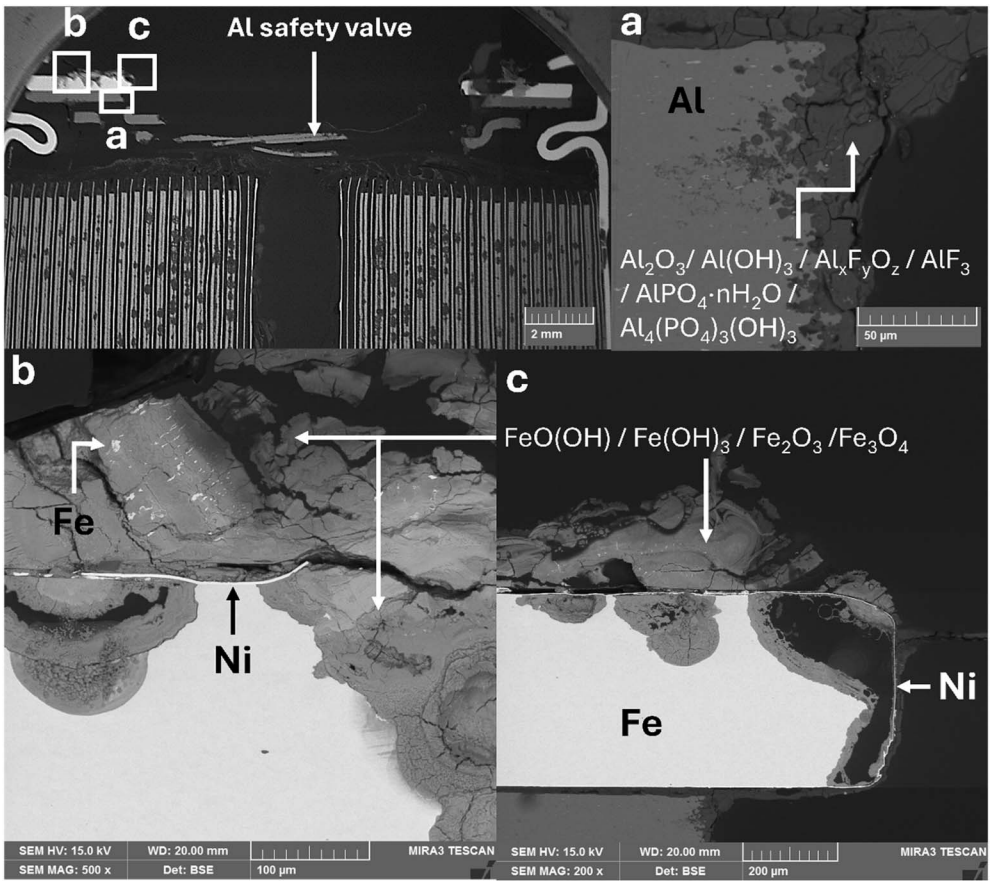

Fig. 4 SEM images of LIB positive terminal cross sections obtained after 23 h discharge in 0.15 m NaCl solution.

solutions originates from the heterogeneity of their surface, creating local domains with negative electric potentials (*i.e.*, anodes) and areas with positive electric potentials (*i.e.*, cathodes). Electrons are released in the anodic process (oxidizing reaction), and they move to the cathodic sites, where neutral or positively charged species can receive them (reduction reaction).[21,22] Considering the species identified during characterization, it is possible that the corrosion mechanism begins as a result of the oxidation of Fe and Ni at the anodic areas according to reactions (3)–(4). When the electrolyte solution contains dissolved oxygen, water reduction takes place at the cathode according to reaction (5).[21,22] These conditions are exacerbated during electrochemical discharge of batteries since O_2 is continuously generated as a product of water splitting (eqn (1)). The formation of O_2 bubbles on the metal surface increases the rate of water reduction reaction (5), while the supply of electric current further promotes the production of OH^- ions by increasing the corrosion current, which accelerates the anodic dissolution of metal.

The Ni^{2+} and Fe^{2+} cations formed by the anodic process combine with the OH^- ions produced by reaction (5) to produce $Ni(OH)_2$ and $Fe(OH)_2$ according to reactions (6)–(8). Fe^{2+} ions produced by anodic dissolution migrate out of the corrosion pits and when the solution contains dissolved oxygen, Fe^{2+} and ferrous (II) hydroxides are oxidized to Fe^{3+} and ferric (III) hydroxides according to reactions (9)–(11).[20,23]

Hydrolysis reactions (12)–(13) of ferric (III) species release H^+ ions, creating acidic solution reservoirs in the imperfections of the oxide and metal surfaces.[20] The hydroxides and oxidic forms of Fe found in the discharge solution and on the steel structures can form from the polymerization and dehydration of ferric (III) hydroxide according to reactions (14)–(16).[20]

In addition to the dissolved oxygen, formation of ferric (III) species accelerates corrosion by creating cathodic reaction sites on the steel surface. Fe^{3+} can undergo reduction, consuming electrons and accelerating the expansion of the pits according to reactions (17)–(18).[23] Additionally, Fe(III) oxides and hydroxides can be reduced on the metal surface, further promoting the corrosion process by consuming the electrons generated during the anodic dissolution of iron according to reactions (19)–(20).[21]

The hydrolysis of Fe^{3+} lowers the pH locally around the pits, with the pH decreasing more sharply as the Fe^{3+} concentration increases due to its stronger hydrolysis ability compared with Fe^{2+}. As the pH drops, the rate of hydrogen gas evolution increases, consuming electrons from the metal surface and raising the corrosion potential.[23] Fe dissolves in acid media since the H_2 gas evolution becomes a thermodynamically favoured cathodic reaction (21).[20]

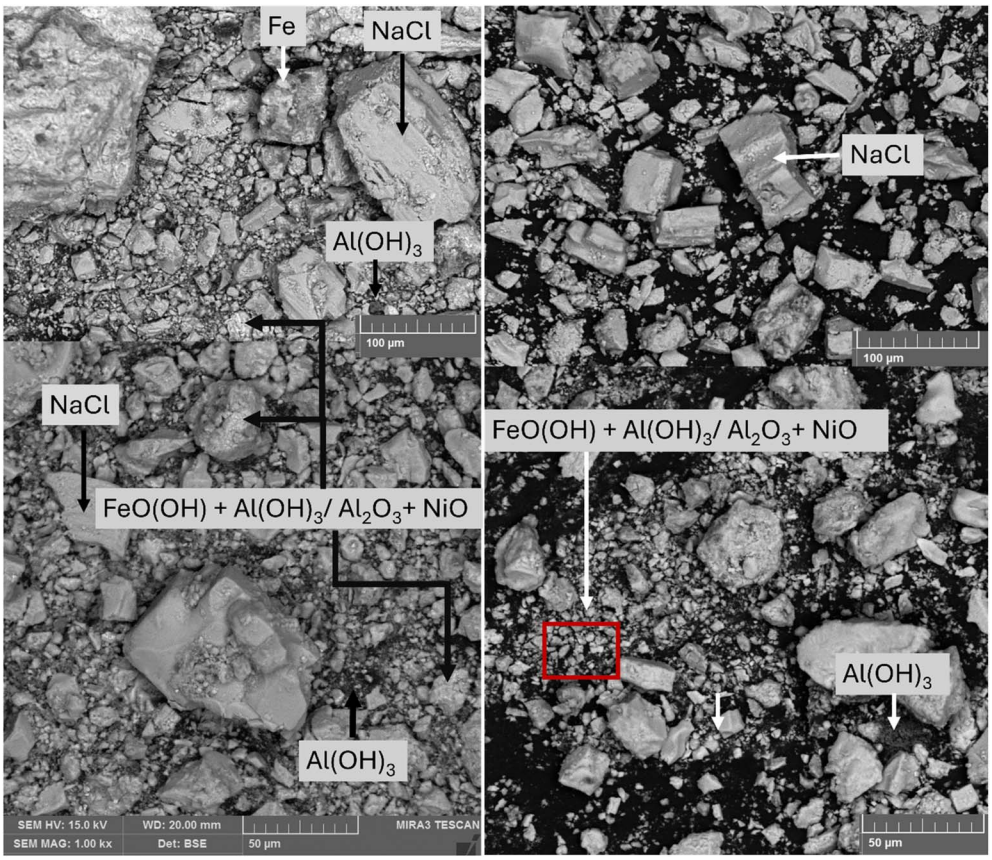

Fig. 5 SEM images of precipitate byproducts obtained from NaCl discharge solutions.

It is also possible that Cl^- ions from the dissolved NaCl salt penetrate oxide scales and metal layers through grain boundaries. Chloride species formation according to reactions (22)–(23) is a spontaneous reaction having a larger negative Gibbs energy of formation compared to oxide formation. The Ni-plating seems to degrade more slowly compared to the steel beneath, which can be explained by the larger negative Gibbs energy of $FeCl_2$ formation compared to $NiCl_2$ formation. Beneath the Ni plating and oxide scales, accumulation of Cl^- ions results in high chlorine partial pressures and low oxygen partial pressures. Under these conditions, metal chlorides become stable.[21,24]

At a certain extent, chloride formation under the Ni-plating creates tensile stresses, mechanically damaging the plating and exposing $FeCl_3$ to water and driving their hydrolyzation according to reactions (24)–(26). This results in the formation of HCl, which accelerates corrosion due to hydrogen reduction reaction (21).[21,22]

During hydrolysis of the chlorine species, the released chlorine diffuses back to the steel surface forming a cycle. Such a cycle facilitates a continuous transport of metals away from the battery casing toward higher oxygen partial pressures in the solution. The total consumption of chlorine is small, thus acting similar to a catalyst for the uncontrolled oxidation of steel.[24]

3.1.2 Corrosion mechanism of the Al safety valve. The EDS analysis of the corroded aluminium safety valve and the corrosion products collected from the discharge solution shown in Fig. 4, 5 and Table S1 indicate the formation of $Al(OH)_3/Al_2O_3$ as corrosion products. The possible electrochemical reactions involving Al-species are collected in Table 3. The corrosion resistance of Al is based on its high reactivity with oxygen, forming a thin Al_2O_3 protective layer. Al_2O_3 has a tight hexagonal close packed crystal lattice created by strong covalent Al–O bonds, which is resistant to formation of lattice defects, creating an effective diffusion barrier between aluminium and its environment.[25] However, if the Al_2O_3 film is damaged under conditions that prevent self-healing of the oxide layer, rapid corrosion ensues.[25]

The positive surface charge of Al_2O_3 attracts Cl^- ions from the NaCl solution to its surface. The suggested mechanism by Nguyen *et al.*[25] by which the Al_2O_3 loses its protective character starts by adsorption of Cl^- on the Al_2O_3 surface, followed by chemical reaction between the Al^{3+} within the hydrated oxide lattice and Cl^- according to reactions (27)–(28). Thus, the oxide scale grows thinner, and the metallic Al is eventually exposed. As shown by the large negative electrochemical potential of reaction (29), Al is highly reactive and ionizes rapidly to Al^{3+}, undergoing rapid hydrolysis according to reactions (30)–(32),[24,26,27] with the oxygen reduction reaction (5) serving as the cathodic counterpart. The intermediate species formed are

Table 2 Corrosion reactions resulting in the degradation of the Ni-plated positive terminal of a cylindrical $LiNi_xCo_yMn_zO_2$ lithium-ion battery

Oxygen generation and water reduction on the metallic surface	
$2H_2O(l) \rightarrow 2H_2(g) + O_2(g)\ E^\circ = 1.23$ V	(1)
$O_2 + 2H_2O + 4e^- \leftrightarrow 4OH^-\ E^\circ = 0.4$ V	(5)
Anodic dissolution of iron and nickel	
$Fe \leftrightarrow Fe^{2+} + 2e^-\ E^\circ = -0.44$ V	(3)
$Ni \leftrightarrow Ni^{2+} + 2e^-\ E^\circ = -0.26$ V	(4)
Oxide formation	
$Ni^{2+} + 2OH^- \rightarrow Ni(OH)_2$	(6)
$Fe^{2+} + 2OH^- \rightarrow Fe(OH)_2$	(7)
$4Fe(OH)_2 + O_2 + 2H_2O \rightarrow 4Fe(OH)_3$	(9)
$Fe(OH)_3 \rightarrow FeO(OH), Fe_3O_4, Fe_2O_3 \cdot nH_2O$	(16)
$Fe^{2+} + H_2O \rightarrow Fe(OH)^+ + H^+$	(8)
$2Fe(OH)^+ + \frac{1}{2}O_2 + 2H^+ \rightarrow 2Fe(OH)^{2+} + H_2O$	(10)
$Fe(OH)^{2+} + H_2O \rightarrow Fe(OH)_2^+ + H^+$	(12)
$Fe(OH)^{2+} + OH^- \rightarrow FeO(OH) + H_2O$	(14)
$2Fe^{2+} + \frac{1}{2}O_2 + 2H^+ \leftrightarrow 2Fe^{3+} + H_2O$	(11)
$Fe^{3+} + H_2O \rightarrow Fe(OH)^{2+} + H^+$	(13)
$Fe(OH)^{2+} + 2OH^- \rightarrow Fe(OH)_3$	(15)
$Fe^{3+} + 3e^- \leftrightarrow Fe\ E^\circ = -0.037$ V	(18)
Active oxidation by chlorine	
$Fe^{2+} + 2Cl^- \leftrightarrow FeCl_2$	(22)
$Fe^{3+} + 3Cl^- \leftrightarrow FeCl_3$	(23)
$FeCl_2 + 2H_2O \rightarrow Fe(OH)_2 + 2Cl^- + 2H^+$	(24)
$FeCl_3 + H_2O \rightarrow Fe(OH)^{2+} + 3Cl^- + H^+$	(25)
$FeCl_3 + 3H_2O \rightarrow Fe(OH)_3 + 3Cl^- + 3H^+$	(26)

highly reactive and soluble in solutions containing H_2O, HCl and NaCl, which promotes a fast corrosion rate.[24]

The exposed Al is attacked by Cl^- according to reactions (33)–(36), forming complexes that rapidly undergo hydrolysis producing a relatively stable $Al(OH)_2Cl$, which is further hydrolysed to $Al(OH)_3$ and HCl according to reactions (37)–(38),[24,26,27] explaining why $Al(OH)_3$ is the final measured corrosion product produced by the dissolution of the aluminium safety valve.

The corrosion rate of the exposed Al surface should be exacerbated by the presence of the more noble Ni used for plating the steel, since Ni and Al are in electrical contact *via* the electrolyte solution. In this case the corrosion of the more active metal is accelerated while the corrosion rate of the more noble metal becomes slower.[20] Fig. 3a and 4b show how the Ni plating is relatively intact while the less noble Fe and Al have extensively corroded away, which is explained by the galvanic corrosion of multimetallic structures.

3.1.3 Interactions between the leaked electrolyte solution and Al safety valve. While the above-described mechanisms can explain the formation of $Al(OH)_3$ as a corrosion product, fluorine and phosphorus were also identified. This indicates interactions with the electrolyte and the conductive lithium hexafluorophosphate ($LiPF_6$) salt, likely due to leakage into the discharging solution. The possible reactions between $LiPF_6$ and the Al safety valve are collected in Table 4.

Table 3 Corrosion reactions resulting in the degradation of the Al safety valve of a cylindrical $LiNi_xCo_yMn_zO_2$ lithium-ion battery

Dissolution of alumina by chlorine	
$Al^{3+}(\text{in } Al_2O_3 \cdot nH_2O \text{ lattice}) + Cl^- \rightarrow Al(OH)_2Cl$	(27)
$Al^{3+}(\text{in } Al_2O_3 \cdot nH_2O \text{ lattice}) + 2Cl^- \rightarrow Al(OH)_2Cl_2^-$	(28)
Oxygen generation and water reduction on the metallic surface	
$2H_2O(l) \rightarrow 2H_2(g) + O_2(g)\ E^\circ = 1.23$ V	(1)
$O_2 + 2H_2O + 4e^- \leftrightarrow 4OH^-\ E^\circ = 0.4$ V	(5)
Anodic dissolution of the exposed Al surface	
$Al \rightarrow Al^{3+} + 3e^-\ E^\circ = -1.66$ V	(29)
Oxide formation	
$Al^{3+} + 3H_2O \rightarrow Al(OH)_3 + 3H^+$	(30)
$Al^{3+} + H_2O \rightarrow AlOH^{2+} + H^+$	(32)
$AlOH^{2+} + Cl^- \rightarrow Al(OH)Cl^+$	(34)
$Al(OH)Cl^+ + H_2O \rightarrow Al(OH)_2Cl + H^+$	(36)
$Al^{3+} + Cl^- \rightarrow AlCl^{2+}/AlCl_2+/AlCl_3$	(33)
$AlCl^{2+} + 2H_2O \vec{O} Al(OH)_2Cl + 2H^+$	(35)
$Al(OH)_2Cl + H_2O \rightarrow Al(OH)_3 + H^+ + Cl^-$	(37)
$2Al(OH)_3 \rightarrow Al_2O_3 \cdot nH_2O$	(38)

Sheng *et al.*[28] have studied the hydrolytic stability of $LiPF_6$ in electrolytes and water showing that $LiPF_6$ is solvated according to reaction (39), greatly improving its hydrolytic stability. The metal and oxide surfaces and especially Al^{3+} ions can activate the decomposition of the PF_6^- ion according to reaction (40).[29]

In a similar fashion to Cl^-, F^- ions diffuse into the Al_2O_3 scale, producing a fluorinated oxide layer with a general formula of $Al_xO_yF_z$ according to reaction (41). The inward

Table 4 Chemical reactions between $LiPF_6$ salt, the discharge solutions and the Al safety valve of a cylindrical $LiNi_xCo_yMn_zO_2$ lithium-ion battery

Solvation of $LiPF_6$	
$LiPF_6 + H_2O \rightarrow Li^+ + PF_6^- + H_2O$	(39)
$PF_6^- \rightarrow P + 6F^-$	(40)
Reactions of Al and F	
$Al^{3+}(\text{in } Al_2O_3 \cdot nH_2O \text{ lattice}) + F^- \rightarrow Al_xO_yF_z$	(41)
$Al^{3+} + 3F^- \rightarrow AlF_3 + 3e^-$	(42)
$Al^{3+} + 6F^- \rightarrow [AlF_6]^{3-} + 3e^-$	(43)
Formation of phosphoric acid	
$P + 2H_2O \rightarrow H_3PO_2 + H^+ + e^-$	(44)
$P + 3H_2O \rightarrow H_3PO_3 + 3H^+ + 3e^-$	(45)
$P + 4H_2O \rightarrow H_2PO_4^- + 6H^+ + 5e^-$	(46)
Solution buffering by phosphoric acid	
$H_3PO_2 + H_2O \rightarrow H_3PO_3 + 2H^+ + 2e^-$	(47)
$H_3PO_3 + H_2O \rightarrow H_3PO_4 + 2H^+ + 2e^-$	(48)
$H_2PO_4^- + H^+ \rightarrow H_3PO_4$	(49)
$H_2PO_4^- \rightarrow HPO_4^{2-} + H^+$	(50)
Formation of phosphates	
$Al(OH)_3 + H_3PO_4 \rightarrow AlPO_4 \cdot 3H_2O$	(51)
$Al(OH)_3 + 3H_3PO_4 \rightarrow Al_4(PO_4)_3(OH)_3 + 6H_2O$	(52)
$Al^{3+} + H_3PO_4 + H_2O \rightarrow AlPO_4 \cdot H_2O + 3H^+$	(53)

diffusion of anions results in formation of corrosion products at the metal/scale interface. The volume expansion creates fractures in the oxide scale, exposing the metal surface to interact with the electrolyte solution.[30] Fluorine can then react with the exposed Al according to reactions (42)–(43).[30,31]

The phosphorus from the PF_6^- ion likely reacts with water producing phosphoric acid (H_3PO_4) according to the Pourbaix diagram of phosphorus at 20 °C (Fig. S3) following reactions (44)–(46).

The dihydrogen phosphate anion $H_2PO_4^-$ has buffering capabilities due to its ability to donate and accept protons. When the pH of the solution decreases, $H_2PO_4^-$ can accept a proton to form H_3PO_4 helping to buffer the system by neutralizing excess H^+ according to reaction (49). When the pH of the solution increases, $H_2PO_4^-$ can lose a proton to form HPO_4^{2-}, helping to buffer by neutralizing excess OH^- according to reaction (50). Consequently, the anodic dissolution rate of metals is reduced in the presence of dihydrogen phosphate ions.[32]

Adsorption of the phosphate ions on the oxide surface creates a diffusion barrier for ion migration between the metal and corrosive solution. In the presence of H_3PO_4, insoluble aluminium phosphates such as $AlPO_4 \cdot nH_2O$ and $Al_4(PO_4)_3(OH)_3$ precipitate in the corrosion pits, where the density of Al^{3+} ions is higher according to reactions (51)–(53). These precipitates cover the anodic dissolution sites, increasing the electrical resistance of the oxide film and reducing the ion exchange in the scale. Phosphorus in the oxide scale has been observed to inhibit crystallization of Al_2O_3, leading instead to formation of an amorphous aluminium phosphate coating. Amorphous films are better diffusion barriers due to the absence of grain boundaries.[32]

The deposition of the leaked electrolyte on the metallic surfaces has likely preserved the remaining metallic pieces on the positive terminal by reducing the oxygen diffusion to the metal surfaces and by the corrosion inhibiting properties of phosphates.

3.2 Corrosion inhibition mechanism by addition of Zn salts

As discussed earlier, the anodic reaction of metal dissolution cannot exist without its pair, the cathodic reaction. In other words, corrosion can be stopped by inhibiting either the anodic or the cathodic side of the corrosion reaction.[20–22]

Anodic corrosion inhibitors increase the polarization of the anode by reaction with cations of the corroding metals to produce diffusion barrier films or salt layers that coat the metal surface and the anodic sites, preventing the interaction with the aggressive environment.[21,22] However, insulating the battery terminals would also prevent its discharge, thus defeating its purpose. Therefore, the approach of cathodic corrosion inhibition is the logical choice in this case.

The protective mechanism of cathodic corrosion inhibitors is based on their reaction with the products of the cathodic electrochemical reaction. The theory says that metals cannot corrode and produce cations faster than the cathode can utilize the electrons, and the electrolyte can transport the current by ionic conduction.[20–22]

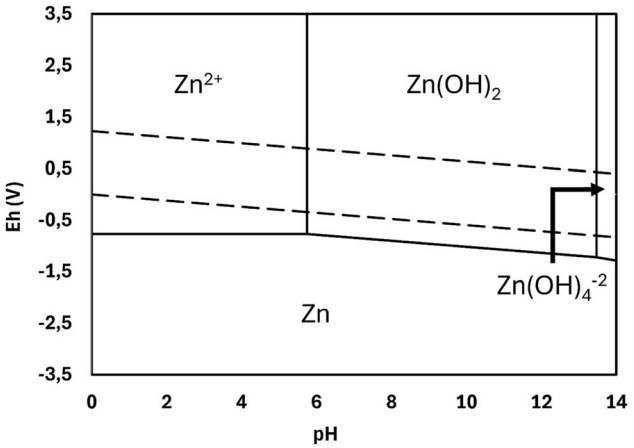

Fig. 6 Pourbaix diagram of zinc calculated with HSC Chemistry at 25 °C, 1 m and 1 bar.

When the electrolyte solution contains dissolved oxygen, the cathodic reaction of oxygen reduction (eqn (5)) produces hydroxyl ions (OH^-). By examining the corrosion reactions of the positive battery terminal in NaCl solution, it is seen that dissolved oxygen in the solution is a prerequisite to several cathodic reactions that accelerate the anodic dissolution of metals. The addition of Zn-containing salts to NaCl solution might prevent most of the cathodic reactions. As shown in the Pourbaix diagram of Zn in Fig. 6, Zn^{2+} forms non-soluble $Zn(OH)_2$ particles according to reactions (54)–(55), consuming the OH^- ions from the system.

$$ZnSO_4 + 2OH^- \rightarrow Zn(OH)_2 + SO_4^{2-} \quad (54)$$

$$ZnCl_2 + 2OH^- \rightarrow Zn(OH)_2 + 2Cl^- \quad (55)$$

These reactions decrease the corrosion rate of both steel and Al-alloys, since oxygen reduction is the dominant reaction responsible for the release of Ni^{2+}, Fe^{2+} and Al^{3+} ions.[21,33–35]

The pH curves recorded during LIB discharging presented in Fig. 7 show that during discharge in NaCl solution, the pH increases due to the production of OH^- and the buffering effect of the dihydrogen phosphate anion $H_2PO_4^-$ formed during leakage of the electrolyte solution. In contrast, the addition of $ZnSO_4$ and $ZnCl_2$ resulted in an acidic solution suggesting that no dissolved OH^- ions are present, likely being consumed by the production of insoluble $Zn(OH)_2$ particles. The formation of $Zn(OH)_2$ particles, which turned into ZnO particles during drying, was also revealed by SEM-EDS analysis of the particles that precipitated in the solution during discharge (SI, Table S2).

The use of $ZnSO_4$ and $ZnCl_2$ in the electrolyte solution resulted in a visibly slower corrosion rate of both the steel terminal and the Al-containing components since these structures remained intact, compared with solutions containing only NaCl (Fig. 8). Despite the good corrosion protection of the metal

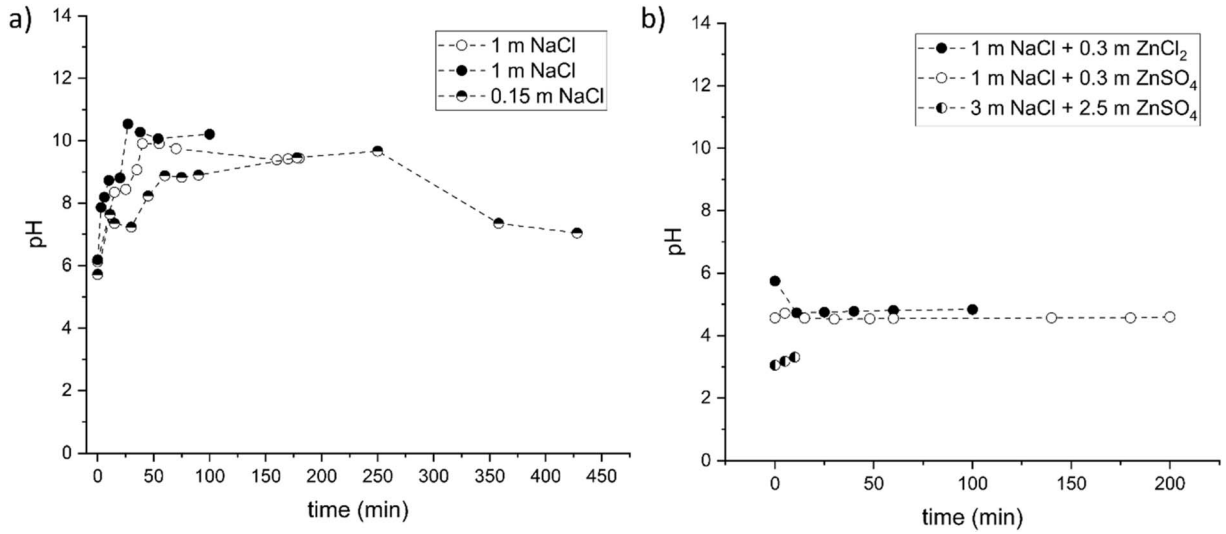

Fig. 7 pH evolution of the electrolyte solutions during discharging of LIBs (a) in NaCl solutions and (b) in NaCl solutions containing $ZnSO_4$ and $ZnCl_2$.

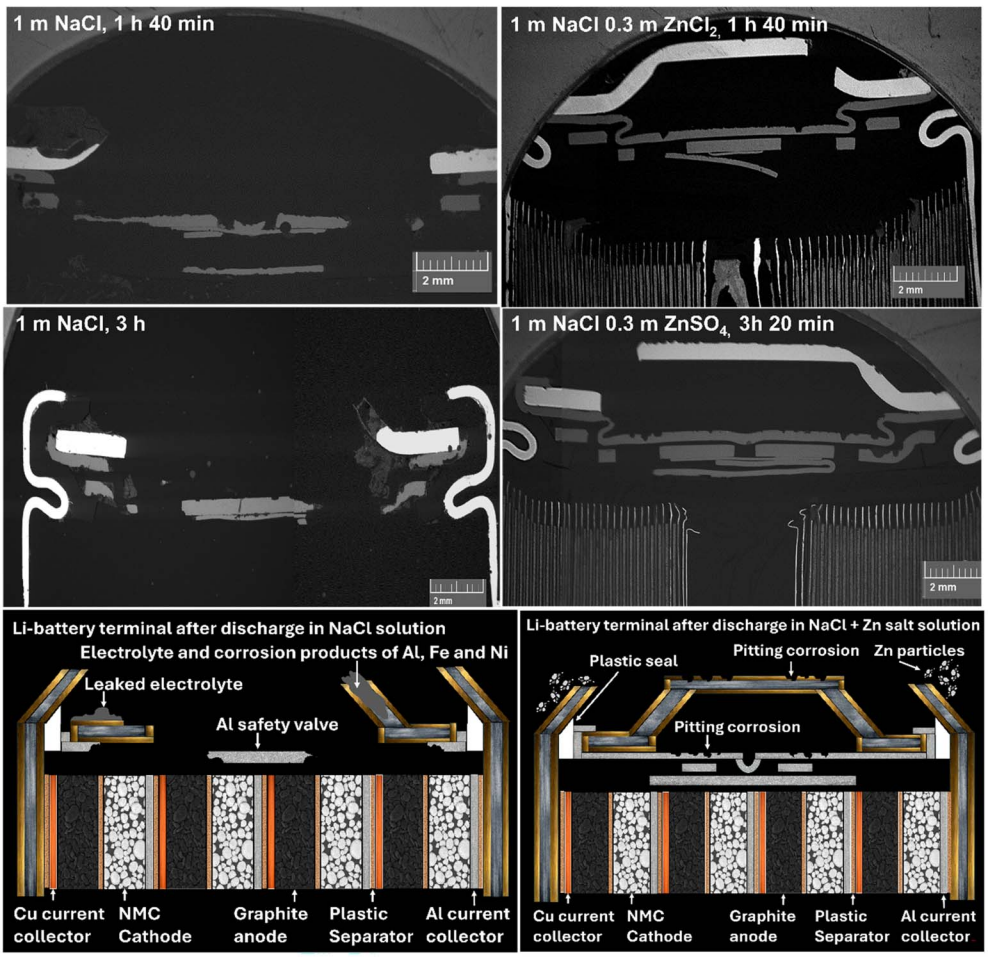

Fig. 8 SEM images of the cross sections of the positive LIB terminals after discharging in 1 m NaCl solution for 1 h 40 min and 3 h and cross sections of discharged LIBs in NaCl + $ZnCl_2$ and NaCl + $ZnSO_4$ solutions after a discharging time of 1 h 40 min and 3 h 20 min, and schematic diagrams of the LIB cross sections representing corroded cross sections after discharge in NaCl and NaCl + Zn salt containing solutions.

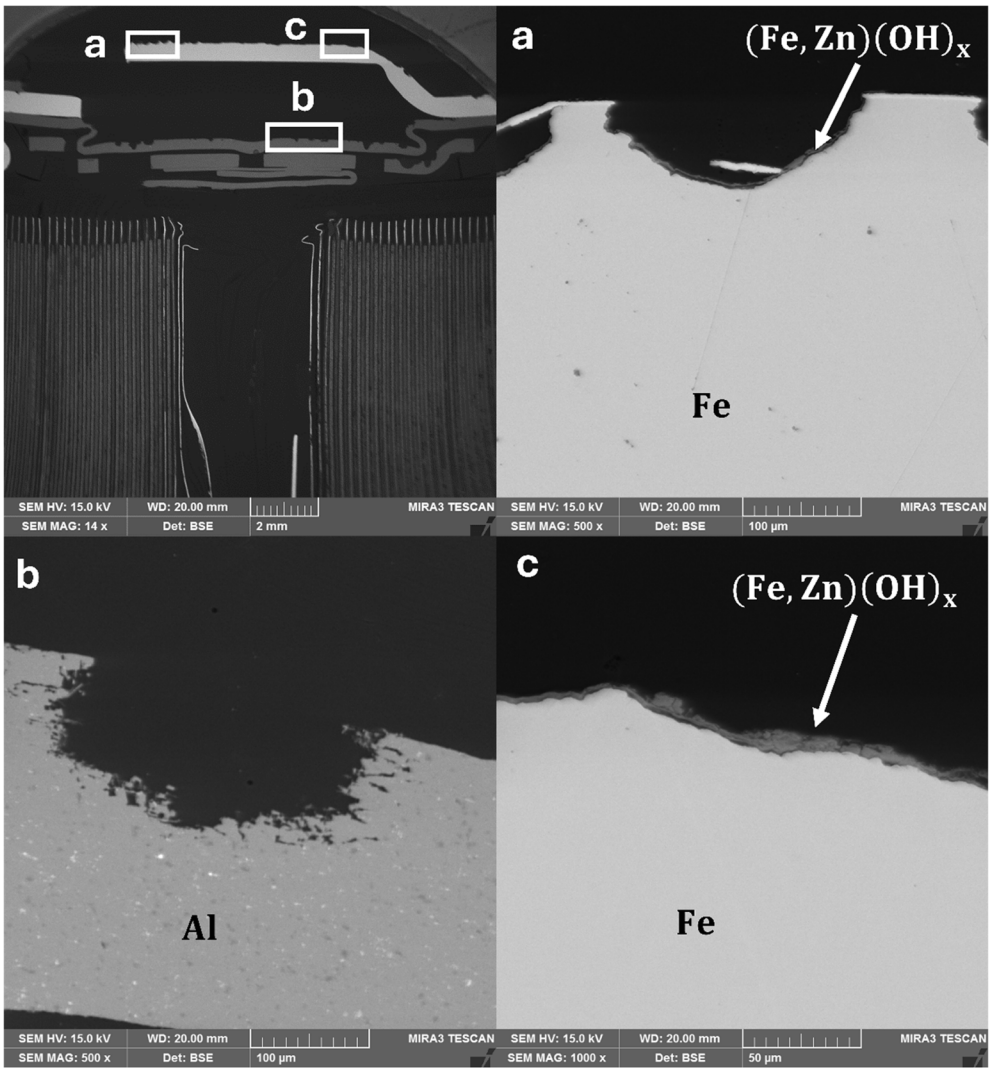

Fig. 9 Scanning electron microscope images of a cross section of a corroded LIB positive terminal in 1 m NaCl + 0.3 m $ZnSO_4$ solution after being kept in the electrolyte solution for 3 hours and 20 minutes.

structures, the plastic sealing ring insulating the positive terminal from the casing described in Fig. 2 got damaged, and some fluorine was detected in the oxide formed in the corrosion pits (Table S2).

Fig. 9a and b show that despite a reduced corrosion rate of the positive terminal with NaCl + $ZnSO_4$ solution, chlorine-induced pitting corrosion was still observed on the Al and steel surfaces. The EDS analysis also shows that Zn^{2+}-ions are incorporated in the oxidic scale inside the pit surface and on the steel surface. Islam *et al.*[33] suggested that $Zn(OH)_2$ could form a chemical bond with the steel oxide scale, while Zn^{2+} could directly bond with the OH^- in the hydrated oxide scale and form a metal cation layer on the oxide surface. Incorporation of Zn^{2+} in the oxide layer covering the anodic areas could decrease the growth rate of pits, providing some protective effect against Cl^- attack by increasing the anodic polarization of the pit.

In acidic environments, the cathodic reaction of H_2 gas evolution (eqn (21)) accelerates the metal dissolution process. H_2 evolution can be controlled by increasing the overvoltage (polarization) of H_2 production by reaction (21), allowing a layer of adsorbed hydrogen to form on the cathodic surface.[20] Here, the $ZnO/Zn(OH)_2$ surface layer could prevent hydrogen gas evolution by adsorbing the hydrogen atoms as indicated by studies of Kokes *et al.*[36] and Usseinov *et al.*[37]

Observations during discharge showed that Zn^{2+} ions deposit on the negative terminal and reduce to metallic Zn according to reaction (56).

$$Zn^{2+} + 2e^- \rightarrow Zn \; E^\circ = 0.76 \text{ V} \quad (56)$$

The composition of metallic Zn particles collected from the electrolyte solution is shown in Fig. 10.

At this point, the chemical reactions of the dissolution of the Ni-plated steel terminal and the Al safety valve have been described. However, there is potentially another mechanism at play in the corrosion process. When the battery is submerged in an electrolyte solution, the Ni-plated steel structure and

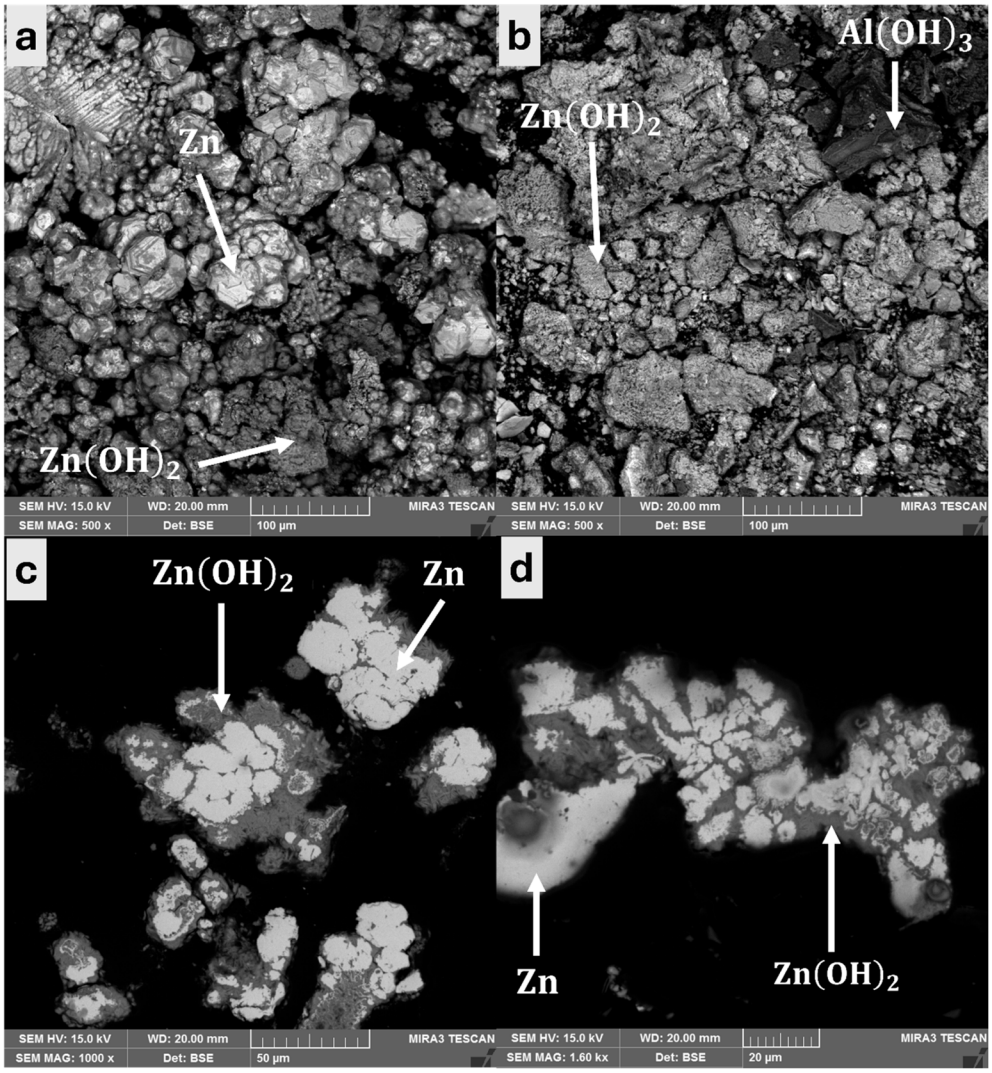

Fig. 10 SEM images of precipitated particles and their corresponding cross sections collected after LIB discharge in NaCl solutions containing $ZnSO_4$.

aluminium safety valve create an electrical circuit *via* the electrolyte. Galvanic corrosion takes place when different metals are coupled to form a wet corrosion cell.[20]

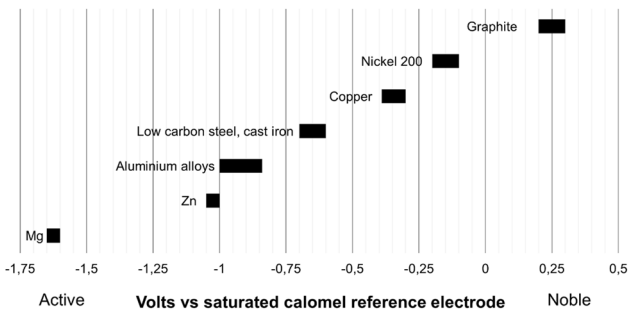

Fig. 11 Free corrosion potentials of alloys used in LIBs measured in flowing sea water at 25 °C. Adapted from Groysman.[21]

Free corrosion potentials of metals and alloys listed in the galvanic series can be used to predict the corrosion tendency of multi-metallic structures. Ideally, the galvanic force series for metals and alloys should be measured separately for every electrolyte solution under specific conditions. Nevertheless, the battery discharge in NaCl solution can be reasonably approximated to the galvanic force series for metals and alloys in flowing sea water at 25 °C shown in Fig. 11.21

According to the theory of galvanic series, the more "active" metal will behave as the anode of the couple in a wet corrosion cell, while the more "noble" metal will act as the cathode. The wider the separation of any two metals in the galvanic series, the more severe the corrosion of the less noble metal will be.[20,21]

The galvanic series shows that formation of metallic Zn during discharging produces a sacrificial anode in the NaCl solution. The battery pole can therefore be protected since all the metals found in the positive terminal act as a cathode while Zn corrodes.[20,22] The oxidized surfaces of the Zn particles in

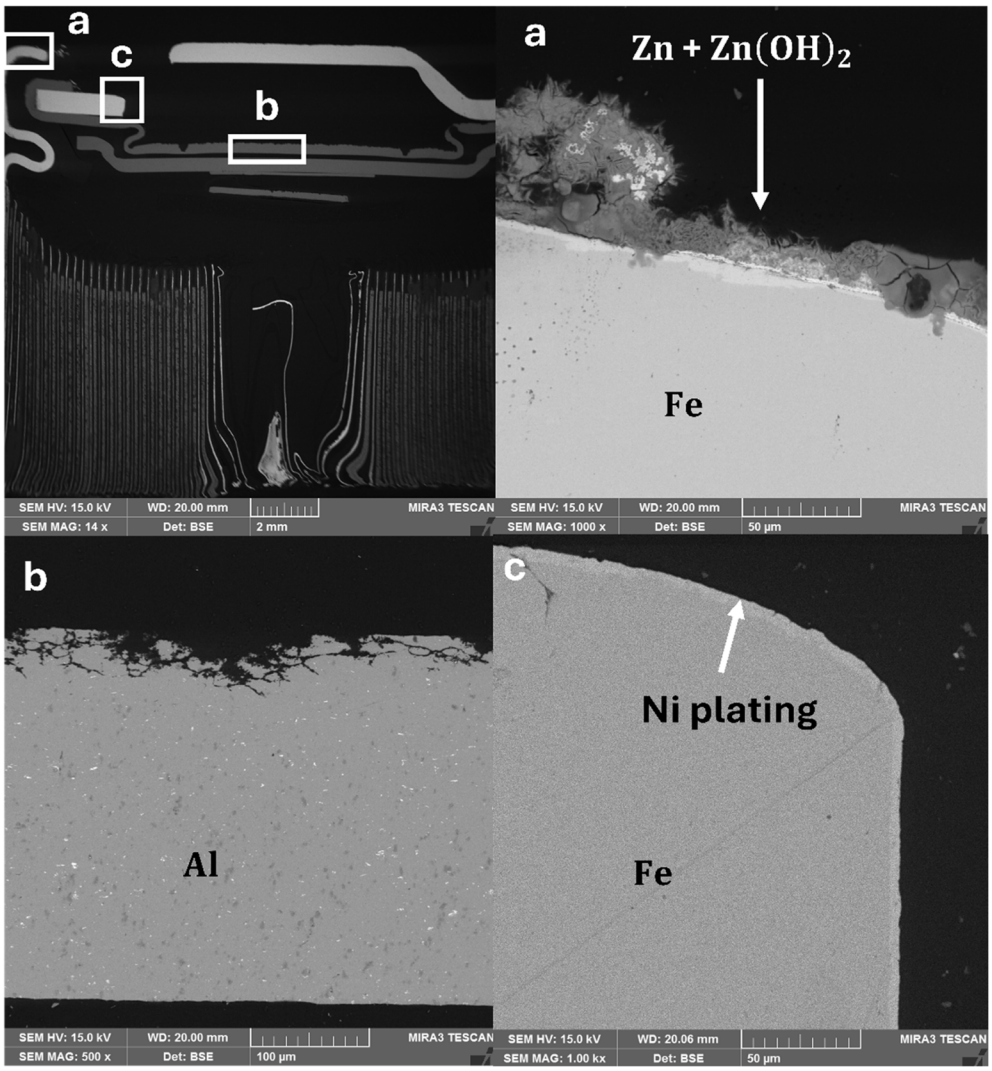

Fig. 12 SEM images of a cross section of the corroded lithium-ion battery positive terminal in 3 m NaCl + 2.5 m $ZnSO_4$ solution after being kept in the electrolyte solution for 15 minutes.

Fig. 10 indicate that the Zn indeed corrodes during the discharging process. This is another explanation for the $Zn(OH)_2$ formation observed during discharging. $Zn(OH)_2$ formation eventually renders the sacrificial anode ineffective. Stronger electrolyte solutions allow a more efficient function of the sacrificial anode because of the higher electrical conductance of the solution.[21] Fig. 12 shows that a strong electrolyte solution produces less pitting corrosion, although the battery was also kept in the solution for only 15 min.

3.3 Discharging performance of NaCl + Zn inhibitor electrolyte solutions

When the battery is submerged in an electrolyte solution, the current conducted between the electrodes encounters electrical resistance and the battery forms an electrical circuit with the electrolyte solution. The electrical energy released by the battery is consumed in various physical, electrical and electrochemical phenomena.[38] As shown in Fig. 13, the addition of $ZnSO_4$ and

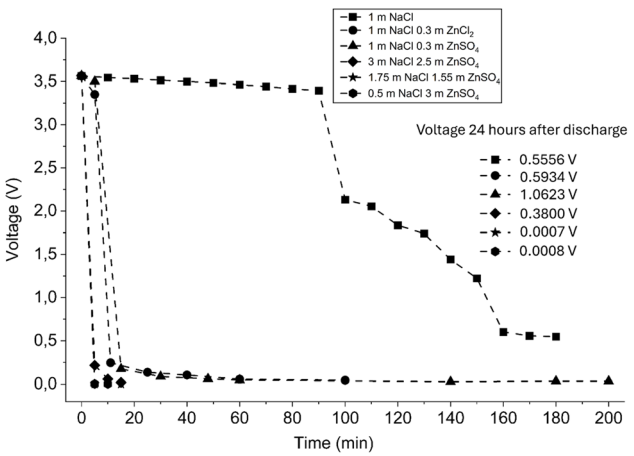

Fig. 13 Discharging rate of LIBs in different electrolyte solutions and final values of voltage relaxation measured 24 hours after the discharge experiments.

$ZnCl_2$ to the NaCl discharge solution resulted in a remarkably fast voltage drop, close to 0 V in 10–15 min, regardless of the concentration of the solution. Both in solutions with and without Zn-salt inhibitors, the voltage relaxation level stayed below 1 V even 24 h after discharge. A higher concentration resulted in lower voltage levels after relaxation, despite having kept the battery in solution for a shorter time (Fig. 13). Full discharge data including voltage relaxation behaviour is presented in SI Fig. S6. Formation of gas bubbles during discharging suggests that the energy from the battery is used to some extent in water splitting according to reaction (1) and potentially hydrogen gas evolution due to acidity of the solutions according to reaction (21).

Ojanen *et al.*[8] increased the discharge rate of LIBs by adding Fe and Zn flakes to Na_2SO_4 and NaCl solutions and explained the increased discharge rate as a result of a larger metallic surface participating in the electrochemical reactions. Similarly, Urtnasan *et al.*[38] discharged LIBs down to 0 V by adding metallic Cu and Fe to an NaCl solution explaining their result of depletion of the battery's voltage down to 0 V by increased electrical resistance resulting in conversion of the battery's energy into heat. Chen *et al.*[19] discharged LIBs to almost 0 V in $CuSO_4$ solution and Fang *et al.*[9] showed that LIBs can be discharged to 0 V when metallic Fe or Zn powders are present in the discharging solution, attributing this phenomenon to a short circuit caused by the metallic powders. Based on the previous research it seems likely that the formation of metallic Zn particles in the solution may have contributed to the fast discharge rate down to almost 0 V since the solution concentration seemed to have no obvious effect on the discharge rate.

The sudden drop in voltage points to an event that is not entirely electrochemical in nature. It was noticed that the battery became warm during discharging, indicating that the energy was partly dissipated as heat. The negatively charged battery casing and the positively charged terminal are close to each other, only separated by the insulating plastic layer.

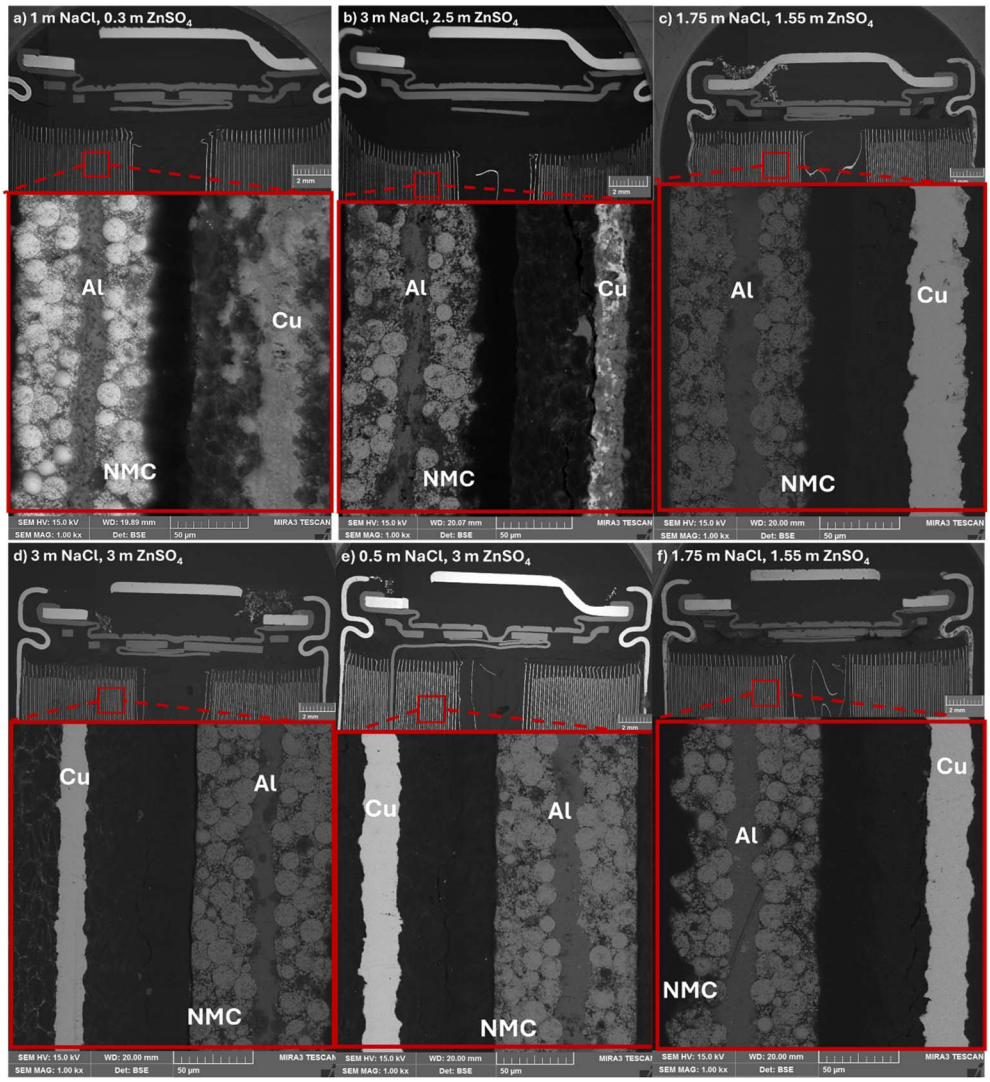

Fig. 14 SEM images showing cross sections of electrochemically discharged LIBs at different NaCl and $ZnSO_4$ concentrations until 0 V and their electrode structures.

Perhaps the metallic powder collecting in the crevices of the positive terminal may have caused an internal short circuit. However, no sparks were observed during the discharge.

Fig. 14 presents SEM images of the cut LIBs after discharge to 0 V at different concentrations of NaCl and $ZnSO_4$. Opening of the battery revealed that sometimes (Fig. 14a and b) the copper current collector was damaged during discharging. However, most samples exhibited no significant structural changes in internal components, such as cathode particles or current collectors (Fig. 14c–f), which indicates that the discharging process does not necessarily compromise their recyclability.

Overdischarging has been observed to cause oxidation of the Cu current collector to Cu^{2+} ions, which can migrate through the separator and reduce at the cathode as metallic copper.[39] In the experiments of this study, copper deposition at the cathode side was not observed. Destruction of the current collectors is unlikely the cause of the voltage drop, since 0 V could also be reached without significant internal damage to the battery.

4 Conclusions

NaCl solution has been extensively studied as a promising electrochemical discharge medium because of its low cost and apparently efficient discharge. However, severe corrosion on the connector poles can lead to incomplete discharging, inaccurate readings of state-of-charge and need for extensive investments in toxic wastewater treatment. Therefore, the objective of this research was to identify the main corrosion mechanisms to propose means of prevention while improving the discharging efficiency.

The corrosion mechanism of the positive battery terminal in NaCl solution showed that dissolved O_2 in the solution and possibly formation of O_2 bubbles on the metallic surfaces due to water splitting combined with electricity provided by the battery increased OH^- production by water reduction on the metallic surfaces. This promoted several parallel cathodic reactions on the metal surface, which resulted in fast and complete anodic dissolution of the positive terminal. Pairing of dissimilar metals in a wet corrosion cell increased the corrosion rate to the extent that the Al safety valve and steel corroded away and allowed the electrolyte to leak to the discharging solution.

To efficiently overcome the corrosion of the battery positive terminal, the use of $ZnSO_4$ and $ZnCl_2$ is herein demonstrated for the first time. Based on the experimental results obtained, it is proposed that the corrosion protection provided by Zn^{2+} ions operates through three mechanisms: (i) Zn^{2+} suppresses the corrosion process by forming non-soluble $Zn(OH)_2$ with OH^- ions produced by oxygen reduction on the metal surfaces; (ii) Zn^{2+} forms a mixed oxide with iron oxide scale on the steel, which can protect the metal by covering anodic areas; and (iii) Zn^{2+} ions consume electrons from the battery forming metallic Zn which acts as a sacrificial anode in the electrolyte solution, being readily corroded instead of the metals at the battery terminals.

The present research demonstrates a cost-effective method for the electrochemical discharge of end-of-life LIBs, improving their safe handling during transportation and recycling. Prevention of thermal runaway in spent batteries results in better separation of the battery materials during mechanical recycling and the mitigation of corrosion contributes to higher recoveries of critical raw materials during LIB recycling since a portion of these elements would otherwise be lost to the discharge solution.

Author contributions

Hanna Sahivirta: conceptualization, data curation, data analysis, writing the original draft. Annukka Santasalo-Aarnio: resources, validation, writing – review and editing. Rodrigo Serna-Guerrero: conceptualization, resources, validation, writing – review and editing.

Conflicts of interest

The authors declare that they have no known competing financial interests or personal relationships that could have appeared to influence the work reported in this paper.

Data availability

The authors declare that the data supporting the findings of this study are available within the article and its supplementary information (SI). Supplementary information: the EDS-analysis of the corrosion products and thermodynamic phase diagrams of the studied chemical systems. See DOI: https://doi.org/10.1039/d6se00009f.

Acknowledgements

This work was supported by the HYPER-SPHERE project (Grant No. 341628), funded by The Research Council of Finland. The authors would also like to thank Camille Garnier and Eeli Klemelä for conducting many of the discharging experiments and Muhammad Touqeer ul Hussnain for sample preparation and SEM imaging.

References

1 C. Mikolajczak, M. Kahn, K. White and R. T. Long, *Lithium-ion Batteries Hazard and Use Assessment*, Springer Science and Business Media, New York, 2012.
2 European Commission Report, *Communication from the Commission to the European Parliament, the Council, the European Economic and Social Committee and the Committee of the Regions, Critical Raw Materials Resilience: Charting a Path towards Greater Security and Sustainability, Brussels, 3.9.2020 COM*, 2020.
3 M. Bruno, S. Fiore and A. Santasalo-Aarnio, Lithium-ion battery recycling pre-processing with electrochemical discharge: Enhancing gas product analysis and pH monitoring, *Clean. Eng. Technol.*, 2025, **26**, 100938, DOI: 10.1016/j.clet.2025.100938.

4 R. Sommerville, J. Shaw-Stewart, V. Goodship, N. Rowson and E. Kendrick, A review of physical processes used in the safe recycling of Li-ion batteries, *Sustain. Mater. Technol.*, 2020, **25**, e00197, DOI: 10.1016/j.susmat.2020.e00197.

5 A. Nedjalkov, J. Meyer, M. Köhring, A. Doering, M. Angelmahr, S. Dahle, A. Sander and W. Schade, Toxic Gas Emissions from Damaged Lithium-Ion Batteries-Analysis and Safety Enhancement Solution, *Batteries*, 2016, **2**(1), 5, DOI: 10.3390/batteries2010005.

6 H. Wang, G. Qu, J. Yang, S. Zhou, B. Li and Y. Wei, An effective and cleaner discharge method of spent lithium batteries, *J. Energy Storage.*, 2022, **54**, 105383, DOI: 10.1016/j.est.2022.105383.

7 L. P. Yao, Q. Zeng, T. Qi and J. Li, An environmentally friendly discharge technology to pretreat spent lithium-ion batteries, *J. Clean. Prod.*, 2020, **245**, 118820, DOI: 10.1016/j.jclepro.2019.118820.

8 S. Ojanen, M. Lundström, A. Santasalo-Aarnio and R. Serna-Guerrero, Challenging the concept of electrochemical discharge using salt solutions for lithium-ion batteries recycling, *Waste Manag.*, 2018, **76**, 242–249, DOI: 10.1016/j.wasman.2018.03.045.

9 Z. Fang, Q. Duan, Q. Peng, Z. Wei, H. Cao, J. Sun and Q. Wang, Comparative study of chemical discharge strategy to pretreat spent lithium-ion batteries for safe, efficient, and environmentally friendly recycling, *J. Clean. Prod.*, 2022, **359**, 132116, DOI: 10.1016/j.jclepro.2022.132116.

10 L. Wu, F. Zhang, Z. Zhang and C. Zhang, Corrosion behavior and corrosion inhibition performance of spent lithium-ion battery during discharge, *Sep. Purif. Technol.*, 2023, **306**, 122640, DOI: 10.1016/j.seppur.2022.122640.

11 D. Amalia, P. Singh, W. Zhang and A. N. Nikoloski, Discharging of Spent Cylindrical Lithium-Ion Batteries in Sodium Hydroxide and Sodium Chloride for a Safe Recycling Process, *JOM*, 2023, **75**, 4946–4957, DOI: 10.1007/s11837-023-06093-x.

12 M. M. Torabian, M. Jafari and A. Bazargan, Discharge of lithium-ion batteries in salt solutions for safer storage, transport, and resource recovery, *Waste Manag. Res.*, 2022, **40**(4), 402–409, DOI: 10.1177/0734242X211022658.

13 H. Rouhi, R. Serna-Guerrero and A. Santasalo-Aarnio, Electrochemical discharge of Li-ion batteries - A methodology to evaluate the potential of discharge electrolytes without corrosion, *J. Energy Storage.*, 2022, **55**, 105734, DOI: 10.1016/j.est.2022.105734.

14 H. Rouhi, E. Karola, R. Serna-Guerrero and A. Santasalo-Aarnio, Voltage behavior in lithium-ion batteries after electrochemical discharge and its implications on the safety of recycling processes, *J. Energy Storage.*, 2021, **35**, 102323, DOI: 10.1016/j.est.2021.102323.

15 J. Xiao, J. Guo, L. Zhan and Z. Xu, A cleaner approach to the discharge process of spent lithium-ion batteries in different solutions, *J. Clean. Prod.*, 2020, **255**, 120064, DOI: 10.1016/j.jclepro.2020.120064.

16 J. Shaw-Stewart, A. Alvarez-Reguera, A. Greszta, J. Marco, M. Masood, R. Sommerville and E. Kendrick, Aqueous solution discharge of cylindrical lithium-ion cells, *Sustain. Mater. Technol.*, 2019, **22**, e00110, DOI: 10.1016/j.susmat.2019.e00110.

17 V. I. Nazarov, V. M. Retivova, D. A. Makarenkova, A. P. Popova, G. R. Aflyatunovaa and N. A. Kuznetsova, Preliminary Discharge of Spent Lithium Batteries in Salt Solution for Safe Disposal, *Coke Chem.*, 2022, **65**, 564–571, DOI: 10.3103/S1068364X22700296.

18 L. Wu, F. Zhang, K. He, Z. Zhang and C. Zhang, Avoiding thermal runaway during spent Li-ion battery recycling: A comprehensive assessment and a new approach for battery discharge, *J. Clean. Prod.*, 2022, **380**, 135045, DOI: 10.1016/j.jclepro.2022.135045.

19 X. Chen, W. Hua, L. Yuan, S. Ji, S. Wang and S. Yan, Evolution fate of battery chemistry during efficient discharging processing of spent lithium-ion batteries, *Waste Manag.*, 2023, **170**, 278–286, DOI: 10.1016/j.wasman.2023.09.005.

20 K. R. Trethewey and J. Chamberlain, *Corrosion for Students of Science and Engineering*, John Wiley and sons, New York, 1988.

21 A. Groysman, *Corrosion for Everybody*, Springer, New York, 2010.

22 D. A. Jones, *Principles and Prevention of Corrosion*, Maximillian publishing company, New York, 1991.

23 H. Zhang, N. Du, S. Wang, Q. Zhao and W. Zhou, Determination of Iron Valence States Around Pits and the Influence of Fe3+ on the Pitting Corrosion of 304 Stainless Steel, *Materials*, 2020, **13**(3), 726, DOI: 10.3390/ma13030726.

24 C. Verma, E. E. Ebenso and M. A. Quraishi, Corrosion inhibitors for ferrous and non-ferrous metals and alloys in ionic sodium chloride solutions, *A review, J. Mol. Liq.*, 2017, **248**, 927–942, DOI: 10.1016/j.molliq.2017.10.094.

25 T. H. Nguyen and R. T. Foley, The Dissolution Mechanism of Aluminum Oxide and Aluminum Powder in Various Electrolytes, *J. Electrochem. Soc.*, 1980, **127**, 2563, DOI: 10.1149/1.2129520.

26 R. T. Foley and T. H. Nguyen, The Chemical Nature of Aluminum Corrosion: V. Energy Transfer in Aluminum Dissolution, *J. Electrochem. Soc.*, 1982, **129**, 464, DOI: 10.1149/1.2123881.

27 R. Padash, A. H. Jafari and E. Jamalizadeh, Experimental and theoretical study of aluminium corrosion in NaOH, NaCl and HCl solutions, *Anti-CorrosMethods Mater*, 2018, **65**(4), 350–360, DOI: 10.1108/ACMM-04-2017-1785.

28 L. Sheng, D. Zhu, K. Yang, Y. Wu, L. Wang, J. Wang, H. Xu and X. He, Unraveling the Hydrolysis Mechanism of LiPF6 in Electrolyte of Lithium-Ion Batteries, *Nano Lett.*, 2024, **24**, 533–540, DOI: 10.1021/acs.nanolett.3c01682.

29 T. Miyashita, K. Yasuda and T. Uda, Kinetics and mechanism of hydrolysis of PF_6^- accelerated by H^+ or Al^{3+} in aqueous solution, *Environ. Sci.: Water Res. Technol.*, 2025, **11**, 281, DOI: 10.1039/D4EW00758A.

30 E. Yoon, J. Lee, S. Byun, D. Kim and T. Yoon, Passivation Failure of Al Current Collector in LiPF6-Based Electrolytes for Lithium-Ion Batteries, *Adv. Funct. Mater.*, 2022, **32**, 2200026, DOI: 10.1002/adfm.202200026.

31 M. Morita, 1, T. Shibata, N. Yoshimoto and M. Ishikawa, Anodic behavior of aluminum in organic solutions with different electrolytic salts for lithium-ion batteries, *Electrochim. Acta*, 2002, **47**, 2787–2793, DOI: 10.1016/S0013-4686(02)00164-0.

32 M. Mohammadi, A. Yazdani, M. E. Bahrololoom and A. Alfantazi, Corrosion behavior of 2024 aluminum alloy anodized in presence of permanganate and phosphate ions, *J. Coat. Technol. Res.*, 2013, **10**(2), 219–229, DOI: 10.1007/s11998-012-9459-x.

33 Md. S. Islam, K. Otani and M. Sakairi, Effects of metal cations on mild steel corrosion in 10 mM Cl^- aqueous solution, *Corros. Sci.*, 2018, **131**, 17–27, DOI: 10.1016/j.corsci.2017.11.015.

34 M. Mahdavian and R. Naderi, Corrosion inhibition of mild steel in sodium chloride solution by some zinc complexes, *Corros. Sci.*, 2011, **53**, 1194–1200, DOI: 10.1016/j.corsci.2010.12.013.

35 K. E. M. Mohamed, O. H. Ibrahim, M. E. El-Bedawy and A. H. Ali, Synergistic effect of different Zn salts with sodium octanoate on the corrosion inhibition of carbon steel in cooling water, *J. Radiat. Res. Appl. Sci.*, 2020, **13**, 276–287, DOI: 10.1080/16878507.2020.1730603.

36 R. J. Kokes, A. L. Dent, C. C. Chang and L. T. Dixon, Infrared Studies of Isotope Effects for Hydrogen Adsorption on Zinc Oxide, *J. Am. Chem. Soc.*, 1972, **28**, 4429–4436.

37 A. B. Usseinov, E. A. Kotomin, A. T. Akilbekov, Yu. F. Zhukovskii and J. Purans, Hydrogen adsorption on the ZnO surface: *ab initio* hybrid density functional linear combination of atomic orbitals calculations, *Phys. Scr.*, 2014, **89**, 045801, DOI: 10.1088/0031-8949/89/04/045801.

38 E. Urtnasan and J.-P. Wang, A Metal Accelerator Approach for Discharging Cylindrical Lithium-Ion Batteries in a Salt Solution, *Metals*, 2024, **14**, 657, DOI: 10.3390/met14060657.

39 A. Kaas, C. Wilke, A. Vanderbruggen and U. A. Peuker, Influence of different discharge levels on the mechanical recycling efficiency of lithium-ion batteries, *Waste Manag.*, 2023, **172**, 1–10, DOI: 10.1016/j.wasman.2023.08.042.